Journal of Petroleum Science and Engineering 209 (2022) 109719

Contents lists available at ScienceDirect

Journal of Petroleum Science and Engineering

journal homepage: www.elsevier.com/locate/petrol

Identification of distinctions of immiscible CO_2 huff and puff performance in Chang-7 tight sandstone oil reservoir by applying NMR, microscope and reservoir simulation

Yongcheng Luo [a,b,c,*], Taiyi Zheng [a,d], Hanmin Xiao [b,c], Xiangui Liu [b,c], Haiqin Zhang [c], Zhenkai Wu [a,b,c], Xinli Zhao [a,b,c], Debin Xia [a]

[a] College of Engineering Science, University of Chinese Academy of Sciences, Beijing, 100049, China
[b] Institute of Porous Flow and Fluid Mechanics, University of Chinese Academy of Sciences, Langfang, 065007, China
[c] Research Institute of Petroleum Exploration & Development, Beijing, 100083, China
[d] Institute of Mechanics, Chinese Academy of Science, Beijing, 100190, China

ARTICLE INFO

Keywords:
CO_2 huff and puff
Nuclear magnetic resonance
Residual oil distribution
Molecular diffusion
Asphaltene precipitation

ABSTRACT

CO_2 huff and puff (HNP) is one of the most effective methods to improve tight oil recovery after the primary depletion process. The seepage mechanisms between CO_2 and crude oil are complicated in porous media during CO_2 HNP process. Therefore, in this paper, the CO_2 HNP process of Chang-7 tight oil reservoir, Ordos Basin, China, was studied by nuclear magnetic resonance (NMR) technology, microscopic observation and numerical simulation. Experimentally, using NMR technology and microscopy methods, the distribution characteristics of residual oil during CO_2 HNP process were measured intuitively. Numerically, a group of core-scale and field-scale simulations considering molecular diffusion and asphaltene precipitation were established to further verify and elongate the experimental results. The results show that at the initial state, the crude oil in the tight core was mainly distributed in nanopores, sub-micro-nanopores and sub-micropores, where the oil content exceeded at least 73% in these pores. During CO_2 HNP process, the oil recovery was more pronounced for the 1st and 2nd rounds than for 3rd to 5th rounds. Notably, even if the cores with more nano-pores were more favorable for the 4–5th CO_2 HNP rounds, the oil molecules in nanopores were still difficult to be available. Moreover, the CO_2 sweep scope could be divided into displacement affected region and diffusion affected region. CO_2 could effectively drive the crude oil in the displacement affected region. While the oil could be successfully displaced by dissolved gas flooding in the diffusion affected region only under the appropriate conditions. Meanwhile, the core-scale numerical models confirmed that it was necessary to consider molecular diffusion and asphaltene precipitation factors, which would make the simulation results in line with the experiment. In terms of the ultimate oil recovery, the field-scale model only considering the diffusion (2.456%) > the model both considering the diffusion and asphaltene (2.436%) > the model without considering the diffusion and asphaltene deposition (2.412%) > the model only considering the asphaltene deposition (2.388%).

1. Introduction

Over the past decade, tight oil has become a hot spot in the global unconventional oil and gas exploration and development due to the mature application of horizontal wells and hydraulic fracturing technology (Wang et al., 2015, 2017; Sun et al., 2019; Hu et al., 2020; Tang et al., 2017). However, oil recovery is still less than 10% in tight oil reservoirs, and an efficient way for improving oil production is required (Song et al., 2020; Ji and Lee, 2019; Zhao et al., 2019). CO_2 huff and puff (HNP) is one of the most effective ways to improve tight oil recovery after the primary depletion process. CO_2 HNP can also mitigate the greenhouse effect by combining with Carbon Capture use and Storage (CCUS) technology (Li et al., 2019a).

The seepage mechanisms between CO_2 and crude oil are complicated in porous media during CO_2 HNP process. CO_2 has strong solubility in crude oil, which is helpful to reduce the crude oil viscosity and the gas–oil interfacial tension. Tang et al. indicated that CO_2 molecules entered micropores more easily than water molecules. Therefore, CO_2

* Corresponding author. College of Engineering Science, University of Chinese Academy of Sciences, Beijing, 100049, China.
E-mail address: luoyongcheng18@mails.ucas.ac.cn (Y. Luo).

https://doi.org/10.1016/j.petrol.2021.109719
Received 25 August 2021; Received in revised form 14 October 2021; Accepted 22 October 2021
Available online 29 October 2021

HNP could even avoid water sensitive effects in water-sensitive reservoirs. Ma et al. (2019) analyzed the remaining oil distribution under different pore diameters using nuclear magnetic resonance (NMR) technology. The results showed that the macro pores and medium pores were the major oil production areas, while the micropores pores rarely produced oil in the first CO_2 HNP round. But in the subsequent HNP rounds, the small pores and micropores gradually became the main oil production areas in turn. Zhu et al. (2021) also pointed that oil recovery of pores with different sizes varied greatly. The oil recovery of macropores was 6–8 times that of micropores, and remaining oil was mainly distributed in micropores. Meanwhile, Bai et al. (2019) conducted CO_2 HNP experiments to research the influence of fractures on oil recovery by using NMR technology. The results revealed that Fractures could significantly increase the CO_2 sweep volume in the cores, and the ultimate oil recovery of fractured cores was approximately 14% higher than that of unfractured cores. Moreover, there are still some controversies about the role of CO_2 diffusion effect in CO_2 HNP process. Sun et al. (2018), Zhu et al. (2020) and Bai et al. (2019) agreed that molecular diffusion was the prime mechanism for distributing gas into the reservoir during the soaking period, which contributed to increasing CO_2-oil contact area and CO_2 sweep volume. While Alfarge et al. (2018) believed that the diffusion mechanism of CO_2 had almost no effect on the performance of CO_2-EOR, especially in the oil reservoirs with fast CO_2 injection speed. Besides, the precipitation of asphaltenes will be detrimental to oil recovery in the CO_2 HNP process. Li et al. (2019a) explained that the settlement and deposition of asphaltenes in reservoir pores could lead to a decrease in reservoir permeability and even change the state of oil on the rock surface, making the reservoir more lipophilic. Shen et al. (Shen and James, 2018) found that asphaltene deposition was the most significant during the first HNP round due to the rapid increase in CO_2 concentration. At present, CO_2 HNP researches of tight oil reservoir mostly focus on oil recovery or the optimization of injection and production parameters, and lack the research on effective displacement of crude oil in different macroscopical core regions and different microscopic pores by CO_2.

In this paper, the CO_2 HNP process of Chang-7 tight oil reservoir, Ordos Basin, China, was mainly studied by NMR experiment and numerical simulation. Experimentally, regular T_2 spectrum was applied to calculate oil recovery of different pore types. Hierarchical T_2 spectrum and microscopic image were applied to obtain CO_2 sweep scope. Numerically, a group of core-scale and field-scale simulations considering molecular diffusion and asphaltene precipitation were established to further contrast and analyse the effect of CO_2 sweep scope on CO_2 HNP performance.

2. Experimental materials and procedures

2.1. Materials

The experimental cores and oil both came from Chang-7 Oilfield. The basic physical properties of cores are shown in Table 1 and Fig. 1. The permeability was below 0.1mD. The porosity was distributed between 8 and 12%. The crude oil viscosity and oil density were respectively about 5 mPa s and 0.84 g/cm^3 under surface condition. Experimental water was prepared with deuterium water with a salinity of 50 g/L, which can eliminate the nuclear magnetic signal during CO_2 HNP process. Experimental gas was carbon dioxide (99.9 mol% CO_2).

Table 1
Basic physical parameters of the core samples.

Core number	Length /cm	Diameter /cm	Permeability /mD	Porosity /%
#1	6.144	2.504	0.0263	10.787
#2	6.643	2.495	0.0670	12.103
#3	6.961	2.506	0.0736	8.218
#4(Centrifugation)	4.797	2.513	0.0328	9.875

2.2. Experimental setup and procedures

The flow chart of CO_2 HNP experiment is shown in Fig. 2. The experimental setup was mainly composed of core holder, displacement pumps (Q5000, Quizix, Tulsa, America), NMR equipment (MacroMR12, Niumag Analytical Company, China) and microscope (AxioScope.A1 Carl Zeiss, Germany). The experimental procedures are described as follows:

Preparation process: (a) Clean the saline water and oil remaining in the cores. (b) Vacuum these selected cores. (c) Saturate the cores with deuterium water in the vacuum bottle, then immerse these cores in deuterium water for more than 5 days. (d) Displace the saturated cores by the formation oil to establish the irreducible water.

CO_2 HNP process: (a) In the injection period, inject CO_2 into the cores with constant injection pressure (10 MPa). Set the gas injection time to 1 h. (b) In the soaking period, stop CO_2 injection. Set the soaking time to 5 h. (c) In the production period, produce the oil with constant outlet pressure (6 MPa). Set the production time to 10 h. (d) Repeat steps (a)-(c) for the CO_2 HNP process until 5 HNP rounds are completed. Record the regular and hierarchical NMR T_2 spectrum data of the cores during the test. Complementally, the injection pressure, production pressure, injection time and soaking time of CO_2 HNP were determined based on field data and previous studies (Sun et al., 2018; Wang et al., 2016; Zhou et al., 2019; Li et al., 2019b).

Microscopic observation process: (a) Using anhydrous slicing method, cut the cores after the CO_2 HNP test into 6 sections. (b) Use sandpaper to smooth the core section, then use N_2 to blow away core debris on the surface. (c) Place the polished flat surface on the microscope observation table, and photograph at 20, 50 times magnification respectively.

3. Experimental results and discussion

3.1. Pore of tight oil sandstone core

The NMR T_2 spectrum has T_2 relaxation time on the horizontal axis and hydrogen nucleus signal value on the vertical axis. The pore radius can be divided directly according to T_2 relaxation time. The smaller the pore, the smaller the T_2 relaxation time. Sketchily, the pores can be divided into nanopores (<5 ms, <0.05 μm), sub-micro-nanopores (5–10 ms, 0.05–0.1 μm), sub-micropores (10–100 ms, 0.1~1 μm), and micropores (>100 ms, >1 μm). The hydrogen nucleus signal value is an intuitive reflection of crude oil. The larger the signal value, the higher the crude oil content. The formula for calculating the change of oil content is shown in Equation (1).

$$P_{oci} = \frac{\sum_{T_{2,min}}^{T_{2,max}} A_{i,j} - \sum_{T_{2,min}}^{T_{2,max}} A_{i,b}}{\sum_{T_{2,min}}^{T_{2,max}} A_{i,o} - \sum_{T_{2,min}}^{T_{2,max}} A_{i,b}} \times 100\% \quad (1)$$

Where P_{oc} is the oil content (%); $T_{2,min}$ and $T_{2,max}$ are the minimum and maximum T_2 relaxation time, respectively (ms); and $A_{i,j}$, $A_{i,o}$ and $A_{i,b}$ are the corresponding signal strength value of NMR T_2 relaxation time curves of saturated oil, the signal strength of oil-bearing NMR after different core experiments, and NMR spectrometer base semaphore, respectively (A/m).

Fig. 3 illustrates the distribution of crude oil in different pore spaces in tight cores at the initial state. Overall, the oil was mainly distributed in nanopores, sub-micro-nanopores and sub-micropores and the oil content exceeded at least 73% in these pores. Moreover, the lower the core permeability, the more oil was concentrated in the nanopores. When the core permeability was about 0.03mD (#1, #4), the crude oil content in the nanopores and sub-micro-nanopores was dominant, and its ratio was about 62%. Dissimilarly, when the core permeability was about 0.07mD (#2, #3), the oil was relatively evenly distributed in

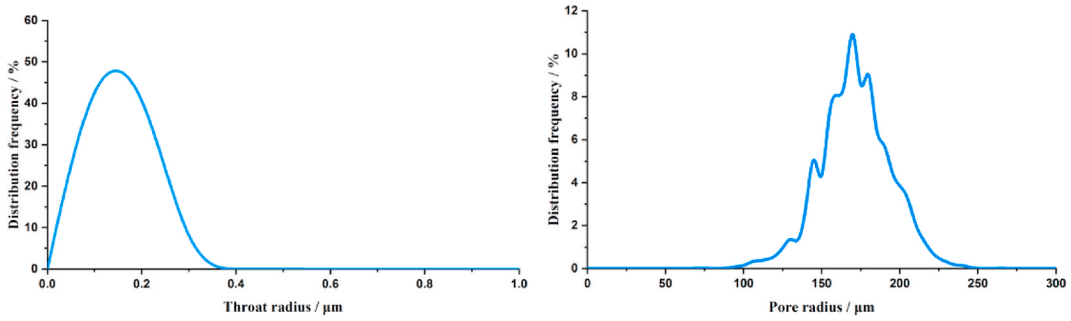

Fig. 1. Pore and throat radius distribution curves.

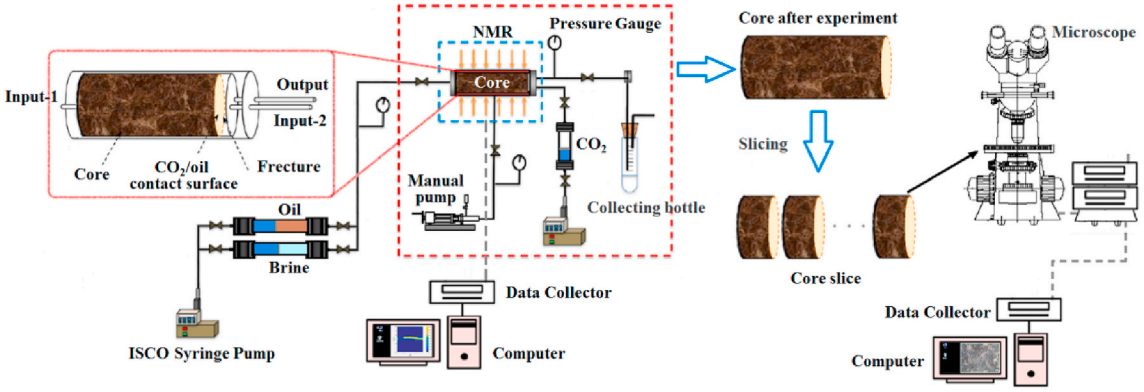

Fig. 2. The flow chart of CO_2 HNP experiment and microscopic observation.

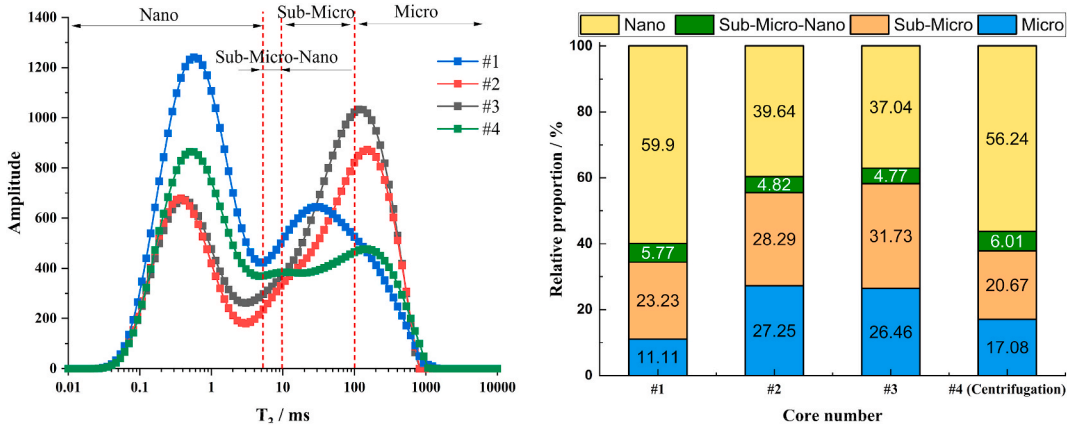

Fig. 3. The distribution of crude oil in tight cores.

nanopores and sub-micro-nanopores (41%), sub-micropores (28%) and micropores (26%).

3.2. Oil recovery characteristics during CO_2 HNP process in tight cores

Fig. 4 shows the NMR T_2 spectrum during CO_2 HNP process in tight cores with different permeability. As can be seen from Fig. 4, crude oil was mainly produced from pores with $T_2 > 5$ ms, while the pores with $T_2 < 5$ ms produced little oil. This experimental result shows that nanopores had a binding effect on oil molecules, which was called the effect of nano-confinement (Song et al., 2020; Liu and Zhang, 2019; Liu et al., 2018). Analogously, the effect of nano-confinement can also be verified by core centrifugal experiments. The NMR T_2 spectrums (Figs. 4 and 5) of centrifugal process and CO_2 HNP process had similar variation characteristics. This result indicated that oil molecules in nanopores were difficult to be moveable either by CO_2 HNP or centrifugation process.

Fig. 6 depicted oil recovery of different tight cores during CO_2 HNP process. According to Fig. 6, the ultimate oil recovery of CO_2 HNP was directly increasing with the permeability, and the oil recovery was more pronounced for the 1st and 2nd rounds than for 3rd to 5th rounds. Pu et al. (2020) pointed that the core permeability was proportional to its pore radius. Under the same external conditions, the large average pore radius would reduce the capillary force and seepage resistance, which could contribute to enhanced oil recovery. In addition, as the HNP round was increased, the oil recovery in low-permeability cores exceeded those in high-permeability cores. Fit the oil recovery of the aforementioned tight cores in rounds 1–5, and the results are as follows:

$$\#1:\ y = 11.216 \cdot x^{(-0.888)} \quad R^{(2)} = 0.9532 \tag{2}$$

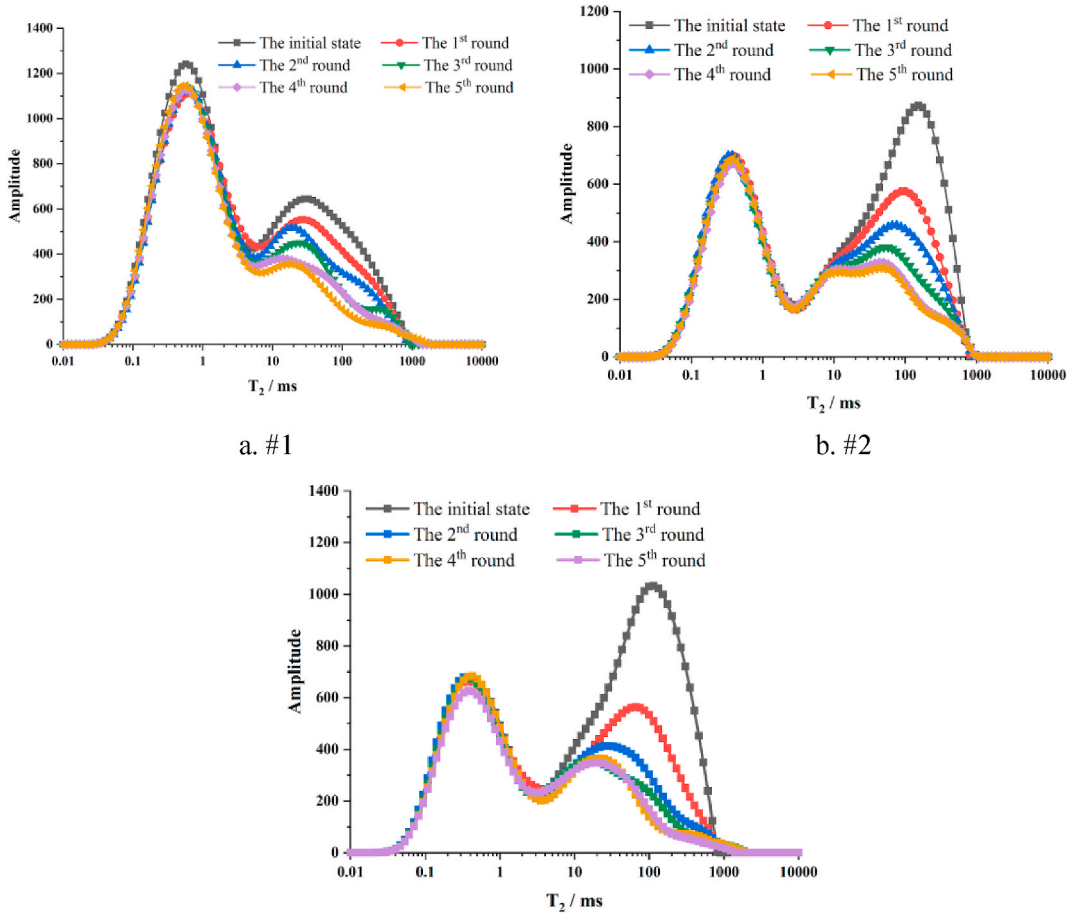

Fig. 4. NMR T_2 spectrum of CO_2 HNP process.

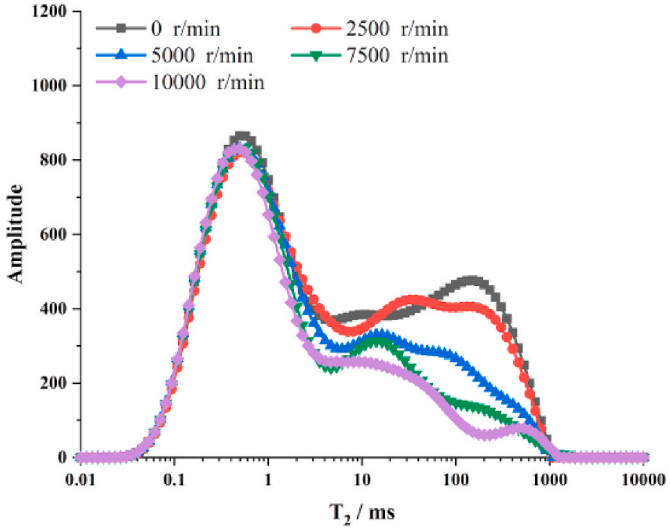

Fig. 5. NMR T_2 spectrum of centrifugal process.

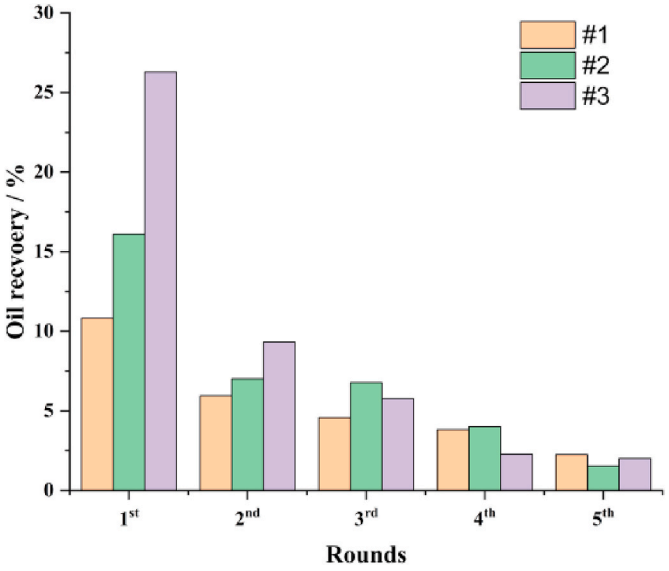

Fig. 6. Oil recovery of different tight cores during CO_2 HNP process.

$$\#2: \ y = 18.089 \cdot x^{(-1.258)} \quad R^{(2)} = 0.8547 \tag{3}$$

$$\#3: \ y = 28.059 \cdot x^{(-1.649)} \quad R^{(2)} = 0.9755 \tag{4}$$

From eqs (2)–(4), the power function index was 1.649 > 1.258>0.888. This illustrated that the oil recovery of cores with relatively large permeability in each HNP round decreased rapidly with the increase of HNP rounds, and vice versa. Specifically, the oil recovery of core #1 in 4–5 rounds (3.81%, 2.25%, respectively) were higher than that of core #3 (2.27%, 2.01%, respectively). It reflected that the cores with more nano-pores were more favorable for the 4–5th CO_2 HNP rounds.

Fig. 7 quantitatively determined the ultimate oil recovery of varying pores during CO_2 HNP process. For low-permeability cores (core #1), the oil recovery of different pore spaces was relatively uniform. Nano-pores and sub-micro-nanopores were 7.55%, sub-micropores was 12.17%, and micropores was 7.69%. While for high-permeability cores (core #3), the sub-micron and micron pores accounted for 92.69% of the total oil recovery. Additionally, after 3 sets of CO_2 HNP experiments, the remaining oil saturation of micropores was only 2.82%–6.14%, the remaining oil saturation of sub-micropores ranged from 11.06% to 14.69%, while the remaining oil saturation of nanopores and sub-micro-nanopores could reach up to 58.11%. The main reasons for the above difference in remaining oil distribution are as follows (Song et al., 2020; Tang et al., 2020; Hawthorne et al., 2013). (1) In the injection process, CO_2 rapidly displaced the crude oil in sub-micropores and micropores and kept it in a movable state. (2) In the soaking period, CO_2 swapped the crude oil in the nanopores and sub-micro-nanopores due to the concentration gradient. CO_2 moved from the gas phase to the oil phase, while light oil components moved from nanopores to sub-micro-nanopores. As the soaking time increased, CO_2 completely penetrated into the nanopores and mixed with the crude oil. As the carbon dioxide expanded further, more oil flowed into the sub-micro-nanopores. (3) In the production process, under the control of production pressure difference, crude oil was preferentially produced from sub-micropores and micropores, and then from nanopores, sub-micro-nanopores to sub-micropores and micropores. From Fig. 8, in the late stage of CO_2 HNP process, the solution gas in nanopores could not overcome the nano-binding effect, which leaded to the decrease of oil production in nanopores. Thus, there were great divergences in the displacement ability of CO_2 to crude oil in different pores of the tight core during HNP process.

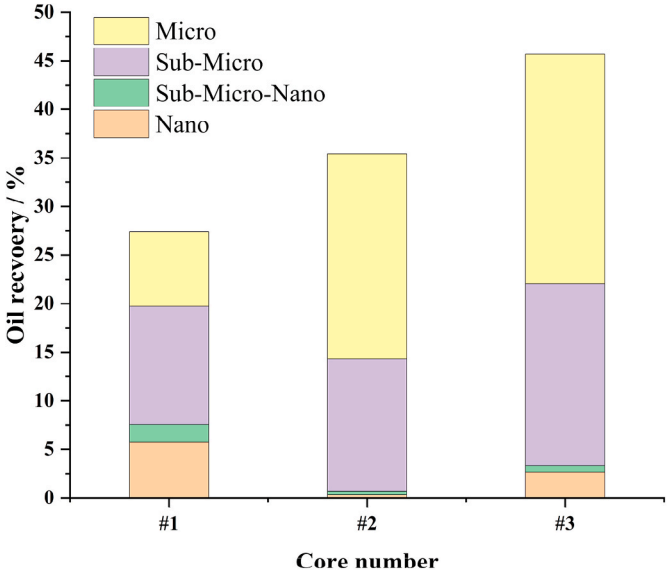

Fig. 7. Ultimate oil recovery of different pores during CO_2 HNP process.

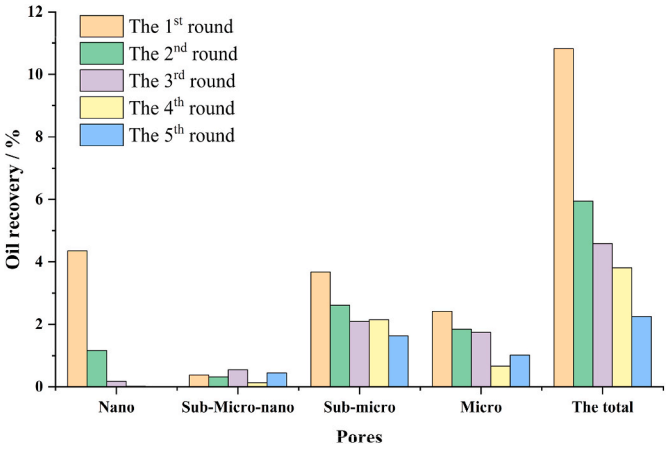

Fig. 8. Oil recovery of core #1 in various pore sizes during CO_2 HNP.

3.3. Microscopic distribution of remaining oil in tight cores during CO_2 HNP process

During the CO_2 HNP process, the hierarchical T_2 spectrum of the core #1 are shown in Fig. 9. It demonstrated the core length on the horizontal axis and the T_2 relaxation time on the vertical axis. From Fig. 9(a), it can be analyzed that the microscopic pore structure was not homogeneous at different positions in the tight sandstone. The pore space at the injection end (the right end) of the core was larger than the other end. From Fig. 9 (b)–9(e), the scope of movable oil spread to the left end of the core as the CO_2 HNP increased. As shown in Fig. 10, there were displacement affected area and diffusion affected area in each CO_2 HNP round, which were primarily and severally determined by pressure difference and molecular diffusion (Tang et al., 2021). The displacement affected area involved significantly more CO_2 than diffusion affected area, which was also close to oil production end. As a result, the CO_2-displaced crude oil production originated mainly from the displacement affected area. Therefore, the transport distance of oil production would increase with increasing of HNP rounds, while the carrying capacity of CO_2 was gradually insufficient, resulting in the effective CO_2 HNP rounds being concentrated in the first two rounds.

Fig. 11 exhibited the microscopic images of core sections at different locations after CO_2 HNP experiment. Sequentially from the right (injection) end to the left end, the surface of the slice core gradually darkened. The oil spot area on the core slice surface was relatively small at the injection end, and it gradually increased as it moved away from the injection end. This indicated that CO_2 could effectively drive the crude oil in the displacement affected area. Whereas the oil couldn't be successfully displaced by dissolved gas flooding in the diffusion affected area, and even numerous heavy components of crude oil such as asphaltene would be generated in the matrix pores, which was not conducive to subsequent development.

4. The numerical model, laboratory to field

4.1. Fluid properties and relative permeability curves

Representative oil components of Chang-7 filed were listed in Table 2 (Zheng et al., 2021a, 2021b). The minimum miscibility pressure (MMP) of CO_2-oil system was predicted via the CMG (a software developed by the Computer Modeling Group) and presented in Fig. 12. Yu et al. (2020) investigated that the MMP ranged from 17.82 MPa to 22.75 MPa for Chang-qing tight oil reservoirs under reservoir condition (64 °C). He et al. predicted that the MMP of Yulin Oilfield were 8.73–17.67 MPa, most of which were between 12–16 MPa (He et al., 2015). Therefore, in this paper, when the simulation environment and injection pressure were severally set to 70.2 °C and 10 MPa, the state of the oil–gas phase

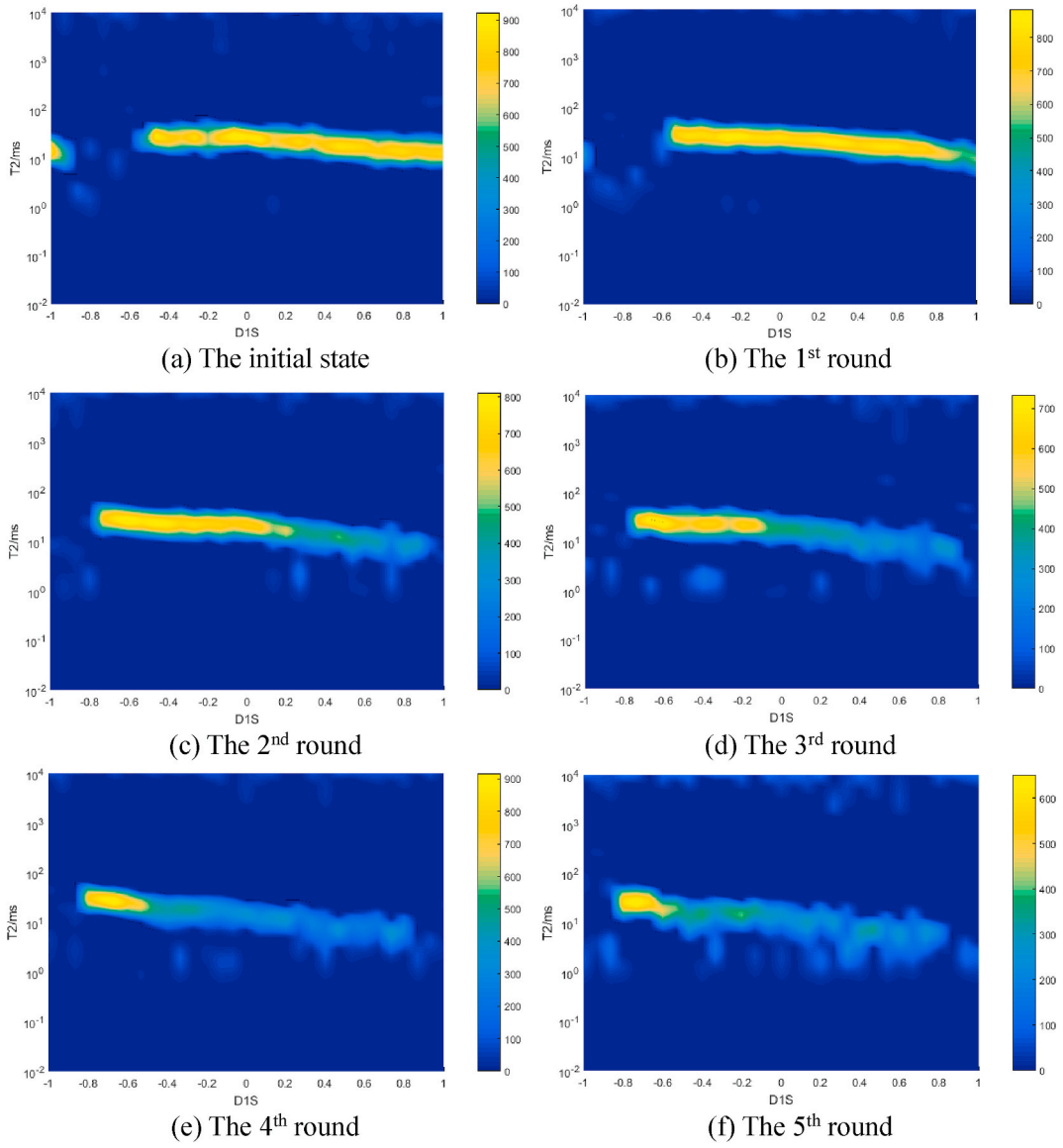

Fig. 9. T_2-SP (hierarchial T_2 spectrum) of the core #1 in 1st to 5th HNP rounds.

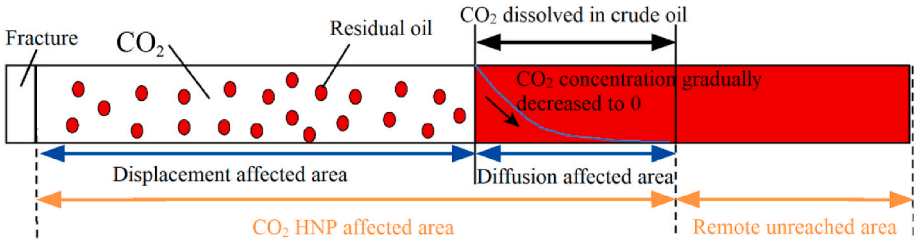

Fig. 10. Schematic of displacement affected area and diffusion affected area (Tang et al., 2021).

was immiscible during the CO_2 HNP process.

According to the experimental result measured by Li et al. (2019c) (Fig. 13), the simulate asphaltene precipitation results with different CO_2 mole fractions via the CMG were presented in Fig. 14. To some extent, both the measured and simulated asphaltene precipitation curves unfolded a peak-like distribution, which was also observed by Shen et al., Syed et al. and Zanganeh et al. (Sun et al., 2018; Syed et al., 2020; Zanganeh et al.,2015, 2018). When the gas injection pressure was lower than the bubble point pressure, the asphaltene precipitation was approximately proportional to the gas injection pressure. While when the gas injection pressure was higher than the bubble point pressure (8.5 MPa), the two were inversely proportional. Moreover, it can be concluded from Figs. 13 and 14 that the amount of asphaltene deposition increased with the CO_2 molar fraction. The relative permeability curves for matrix and fracture were shown in Fig. 15.

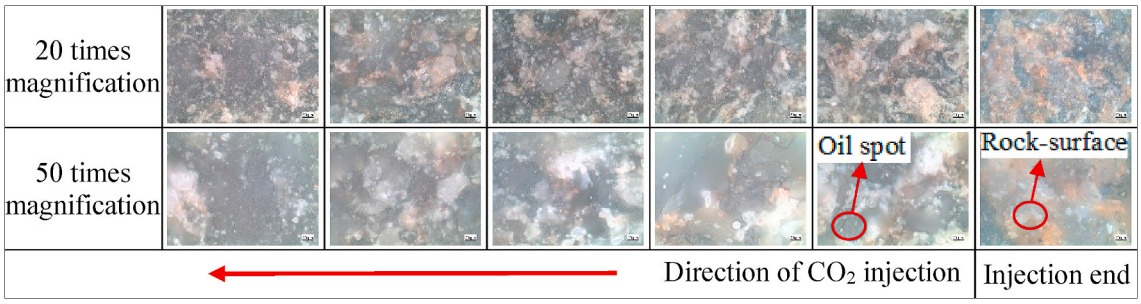

Fig. 11. Microscopic images of core sections at different locations after CO_2 HNP experiment (core #1).

Table 2
Oil components of Chang-7 filed.

Components	Molar fraction	Components	Molar fraction
N_2	0.765	NC_5	1.937
CO_2	0.088	C_6	3.456
C_1	20.094	C_7	5.207
C_2	7.957	C_8	2.521
C_3	10.407	C_9	5.572
IC_4	1.560	C_{10}	3.330
NC_4	4.343	C_{11}	31.252
IC_5	1.510		

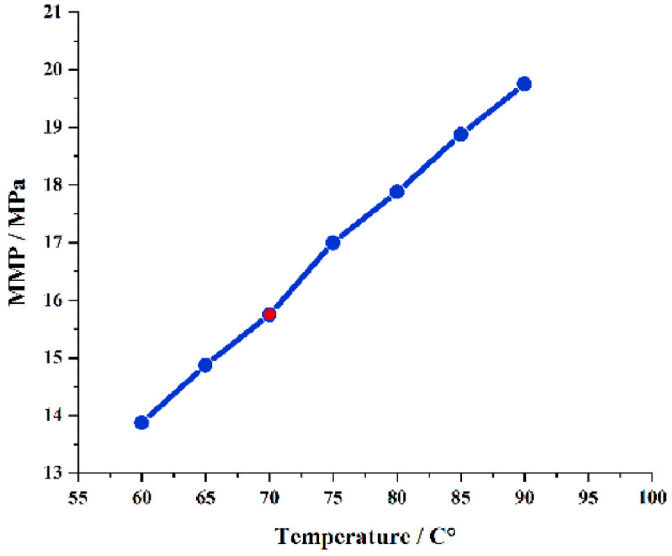

Fig. 12. Miscible pressure at different temperatures.

4.2. Modeling of laboratory experiments

Using CMG to simulate the CO_2 HNP experiment, the 0.0263 mD cylindrical core was equivalently simplified into 6 × 1 × 1 Cartesian grid blocks, where the grid block size were 1.025 × 2.23 × 2.23 cm. Fig. 16 illustrated a schematic diagram of the core-scale numerical modeling. The injector and producer were arranged and overlapped at grid (1,1,1). The crucial parameters related to the model were listed in Table 3.

A numerical mode considering CO_2 diffusion and asphaltene precipitation was established to further confirm experimental results. The numerical model conditions were basically consistent with the experiment, where the gas injection pressure was 10.0 MPa and the time for primary depletion, injection, soaking, and production was 10 h, 1 h, 5 h, and 10 h, respectively. The CO_2 HNP simulation results compared with CO_2 HNP test are shown in Fig. 17. According to the simulation results, the oil recovery in the 1st to 5th rounds was 10.71%, 6.53%, 3.26%,

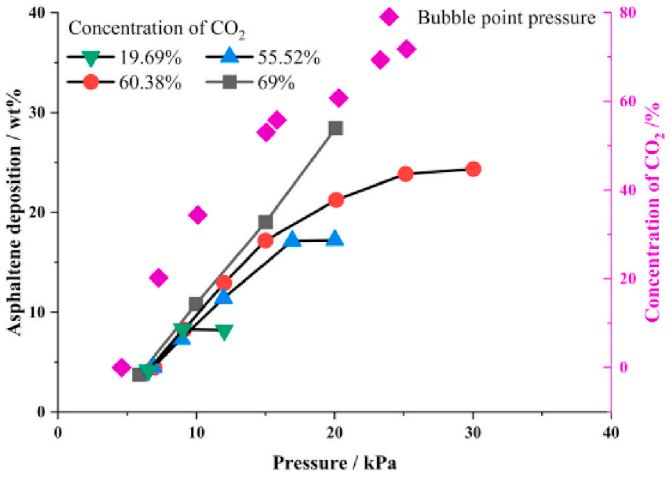

Fig. 13. The relationship curve between relative asphaltene deposition and injection pressure (Li et al., 2019c).

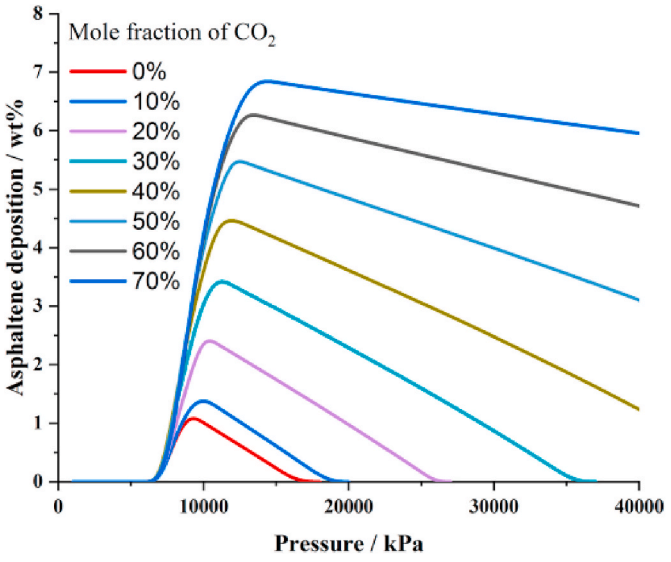

Fig. 14. The amount of asphaltene deposition under different CO_2 mole fraction ratios.

2.68%, 2.20%, respectively. Furthermore, the oil recovery decreased from the 1st round through 5th round, with an inflection point in cycle 3 and low value thereafter. Therefore, the effective HNP rounds were concentrated in the 1st to 3rd rounds, while the 4th and 5th cycles were invalid.

Fig. 18 and Fig. 19 intuitively clarify the residual oil saturation

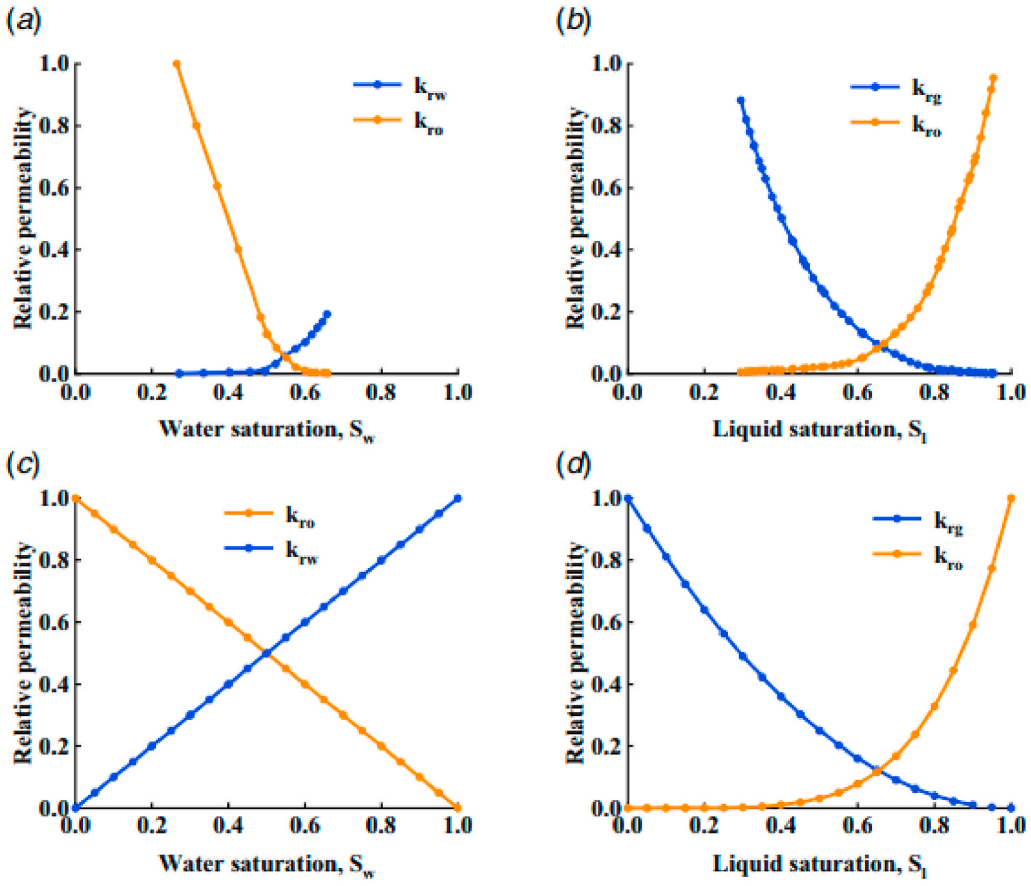

Fig. 15. Relative permeability curves: (a) and (b) matrix (c) and (d) fracture (Zheng et al., 2021a, 2021b).

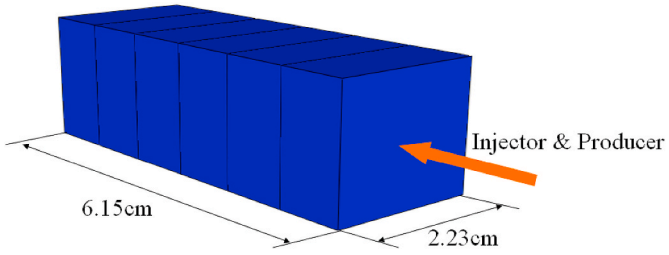

Fig. 16. The schematic core scale model.

Table 3
Fundamental numerical parameters (core #1).

Parameter	Value	Unit
Initial formation pressure	15	MPa
Initial water saturation	30.01	%
Initial oil saturation	69.99	%
Core temperature	72.2	°C
CO_2 diffusion coefficient	2.98×10^{-7}	$m^2 \cdot s^{-1}$
Rock compressibility	0.0007	MPa^{-1}
Matrix permeability	0.0263	mD
Matrix porosity	10.787	%
Primary depletion time	10	hour
Injection time	1	hour
Soaking tine	5	hour
Production	10	hour

distribution during CO_2 HNP process, which were consistent with the residual oil distribution shown in the preceding hierarchical T_2 spectrum. On the whole, the sweep depth of CO_2 was positively correlated with the HNP round. And the CO_2 swept depth was also connected with the displacement affected area and diffusion affected area. When CO_2 molecular diffusion and asphaltene precipitation effects were not involved in the model (Fig. 17), the displacement affected area was limited. Even after 5th HNP rounds, there were effectively still two grids left without touching CO_2. Oppositely, CO_2 could spread to the entire core area quickly when CO_2 molecular diffusion and asphaltene precipitation effects were considered in the model (Fig. 19). Thus, it is necessary to consider molecular diffusion and asphaltene precipitation factors when building numerical models, which will make the simulation results in line with the experiment.

4.3. Modeling of field production

Fig. 20 illustrated a schematic diagram of the field-scale numerical modeling. In order to reduce the calculation cost, the complete horizontal well fracture model (Fig. 20(a)) was tailored into a fracture zone (Fig. 20(b)). The field-scale numerical modeling was composed of a 21 × 101 × 5 Cartesian grid blocks, in which the main fracture was subdivided into 7 × 5 × 1 grids by local grid refinement method. The crucial parameters related to the model were listed in Table 4.

The field-scale model inherited the pivotal parameter setting of the core-scale model with mainly the modification of the production regime. Specifically, the gas injection pressure was 15.0 MPa and the time for primary depletion, injection, soaking, and production was respectively 1year, 1 month, 1 month, and 6 months. Fig. 21 and Fig. 22 illustrates the simulation results of 4 parallel CO_2 HNP field-scale models with or without considering CO_2 diffusion and asphaltene. In terms of the ultimate oil recovery, the model only considering the diffusion (2.456%) > the model both considering the diffusion and asphaltene (2.436%) > the model without considering the diffusion and asphaltene

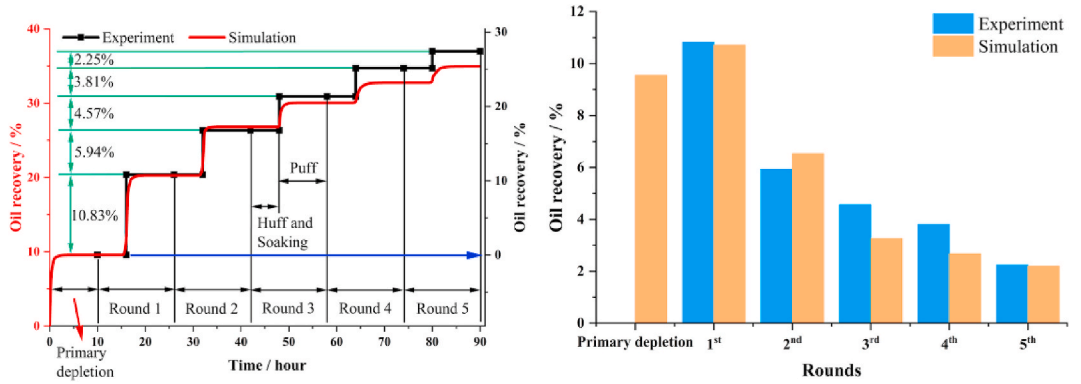

Fig. 17. The CO_2 HNP simulation results compared with CO_2 HNP test.

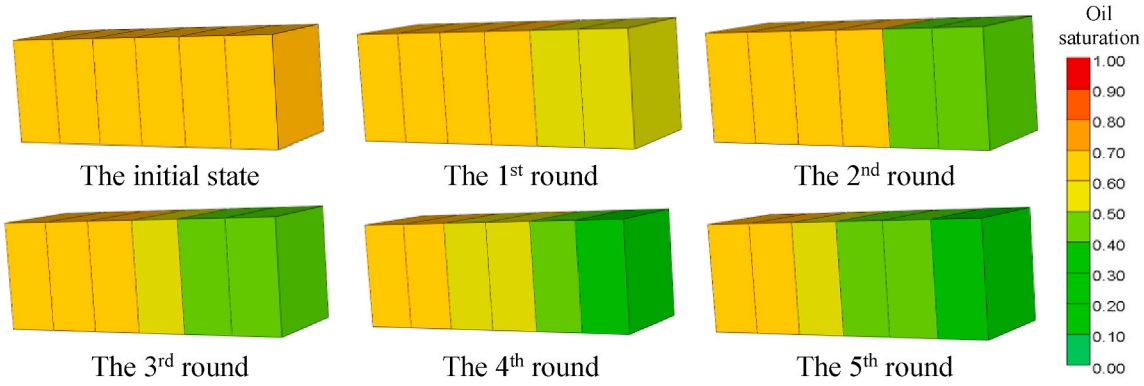

Fig. 18. Residual oil saturation distribution (without considering CO_2 diffusion and asphaltene precipitation).

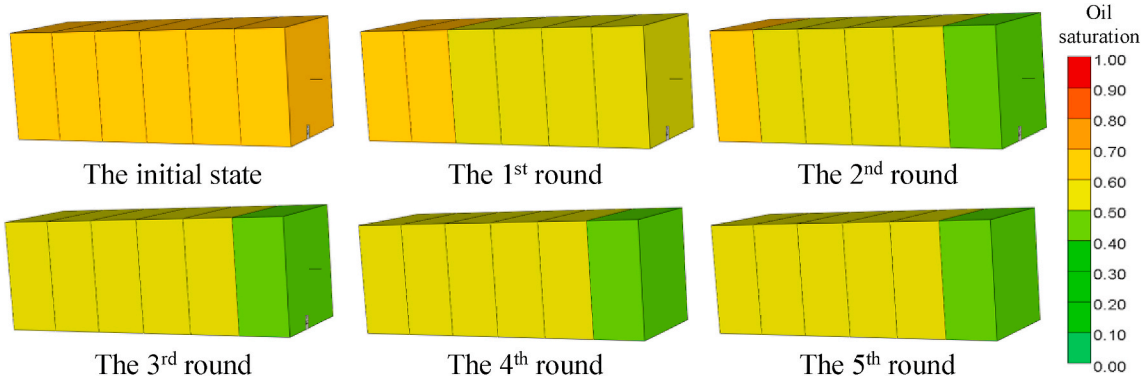

Fig. 19. Residual oil saturation distribution (with considering CO_2 diffusion and asphaltene precipitation).

deposition (2.412%) > the model only considering the asphaltene deposition (2.388%). It can be seen that CO_2 diffusion was beneficial to CO_2 HNP process, while asphaltene deposition was unfavorable. Moreover, the oil recovery of 2 cases considering CO_2 diffusion was obviously higher than the others, especially in the 2nd and 3rd HNP rounds. This was chiefly because the crude oil was derived from region near the fracture and mainly regulated by CO_2 flooding in the initial CO_2 HNP period. Into the middle CO_2 HNP period, the oil-producing region gradually moved away from the fracture area and expanded towards the far end of the reservoir. At this period, the effect of CO_2 diffusion was highlighted to appear. As the CO_2 HNP process continued, the oil-producing region reached the far end of the reservoir, where the crude oil was intractable to migrate out. In addition, Fig. 23 demonstrated gas volume in reservoir and cumulative gas-oil ratio during CO_2 HNP process. From Fig. 23, the gas volume and cumulative gas-oil ratio grown in tandem with HNP round. Under the same production conditions, the models with diffusion had more gas injection volume and lower gas-oil ratio. This further proved that diffusion contributed to the improvement of CO_2 utilization during HNP process.

5. Conclusion

In this paper, experimental and numerical simulation methods were applied to study the seepage characteristics of CO_2 HNP process in tight oil reservoir. Experimentally, using NMR technology and microscopy methods, the distribution characteristics of residual oil during CO_2 HNP process were measured intuitively. Numerically, a group of core-scale and field-scale simulations considering molecular diffusion and asphaltene precipitation were established to further verify and elongate the experimental results. The following research outcomes were

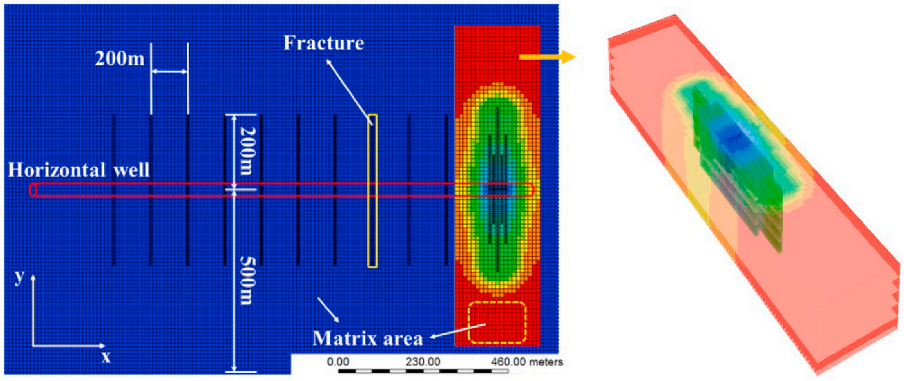

Fig. 20. The schematic field-scale model.

Table 4
Fundamental physical parameters.

Parameter	Value	Unit
Grid number	21 × 101 × 5	/
Grid step size	10 × 10 × 3.2	m
Initial formation pressure	18	MPa
Initial water saturation	30.01	%
Initial oil saturation	69.99	%
Reservoir temperature	72.2	°C
CO_2 diffusion coefficient	2.98×10^{-7}	$m^2 \cdot s^{-1}$
Rock compressibility	0.0007	MPa^{-1}
Matrix permeability	0.0263	$\times 10^{-3} \mu m^2$
Matrix porosity	10.787	%
Effective permeability of main fracture	45	$\times 10^{-3} \mu m^2$
Main fracture width	0.2	m
Primary depletion time	360	day
Injection time	30	day
Soaking tine	30	day
Production	180	day

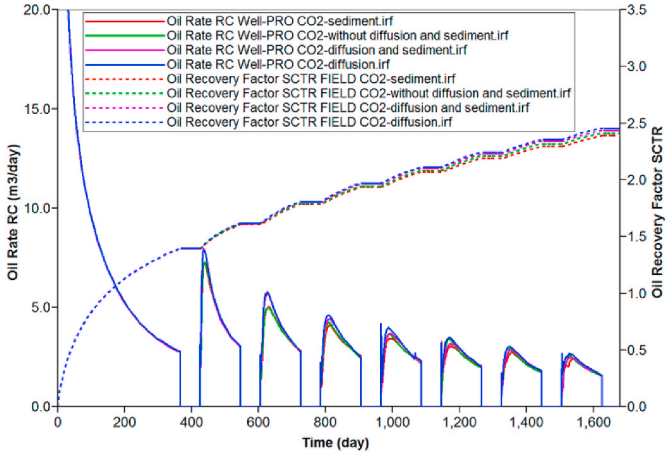

Fig. 21. Daily oil production and cumulative oil recovery.

highlighted:

(1) During CO_2 HNP process, the oil recovery was more pronounced for the 1st and 2nd rounds than for 3rd to 5th rounds. As the HNP round was increased, the oil recovery in low-permeability tight cores exceeded those in high-permeability tight cores. Even if the low-permeability tight cores with more nano-pores were more favorable for the 4–5th CO_2 HNP rounds, the oil molecules in nanopores were still difficult to be available due to the nano-constraint effect.

(2) The CO_2 sweep scope could be divided into displacement affected region and diffusion affected region, which were severally determined by pressure difference and molecular diffusion. The scope of movable oil spread from the gas injection end to the

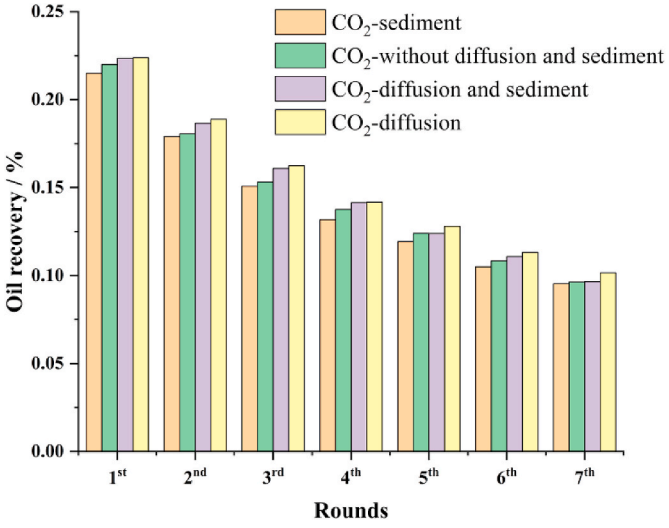

Fig. 22. Oil recovery of each round of field-scale model with different factors.

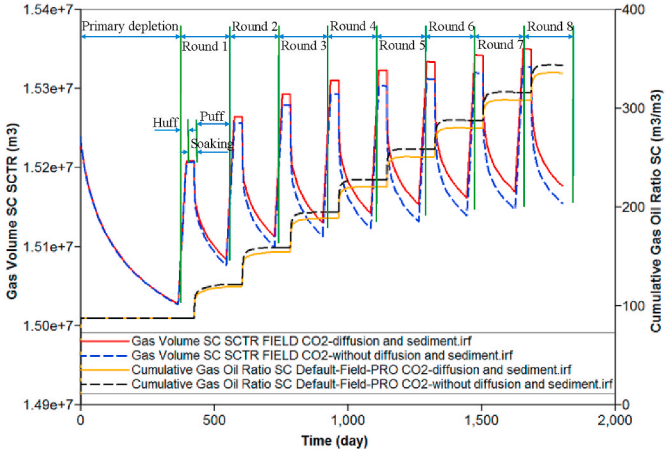

Fig. 23. Gas volume in reservoir and cumulative gas-oil ratio per round.

other end of the core as the CO_2 HNP increased. During this period, CO_2 could effectively drive the crude oil in the displacement affected region. While the oil could be successfully displaced by dissolved gas flooding in the diffusion affected region only under the appropriate conditions.

(3) Apart form HNP rounds, the CO_2 displacement area was associated with CO_2 diffusion and asphaltene precipitation. Under the same production conditions, the model considering the above factors had more contacting area with CO_2. The core-scale numerical models had confirmed that it was necessary to consider molecular diffusion and asphaltene precipitation factors, which would make the simulation results in line with the experiment. Upgrade the model scale from laboratory to field. In terms of the ultimate oil recovery, the field-scale model only considering the diffusion (2.456%) > the model both considering the diffusion and asphaltene (2.436%) > the model without considering the diffusion and asphaltene deposition (2.412%) > the model only considering the asphaltene deposition (2.388%).

Credit author statement

Yongcheng Luo*: Conceptualization, Writing-Original Draft, Investigation, Methodology, Data Curation, Formal analysis, Visualization. **Taiyi Zheng:** Writing-Review & Editing, Validation. Investigation. **Hanmin Xiao**: Resources, Funding acquisition, Supervision. **Xiangui Liu**: Project administration. **Haiqin Zhang**: Writing - Review & Editing. **Zhenkai Wu**: Writing - Review & Editing. **Xinli Zhao**: Writing - Review & Editing. **Debin Xia**: Writing - Review & Editing.

Declaration of competing interest

The authors declare that they have no known competing financial interests or personal relationships that could have appeared to influence the work reported in this paper.

Acknowledgements

This work was supported by the CNPC basic advanced reserve technology (2021DJ2201). This work was also supported in part by the Natural Science Foundation of Chongqing under Grant cstc2020jcyj-msxmX0216, and in part by the Bayu Scholars Program.

References

Alfarge, D., Wei, M., Bai, B., 2018. CO_2-EOR mechanisms in huff-n-puff operations in shale oil reservoirs based on history matching results. Fuel. https://doi.org/10.1016/j.fuel.2018.04.012.

Bai, H., Zhang, Q., Li, Z., Li, B., Zhu, D., Zhang, L., Lv, G., 2019. Effect of fracture on production characteristics and oil distribution during CO_2 huff-n-puff under tight and low-permeability conditions. Fuel. https://doi.org/10.1016/j.fuel.2019.02.107.

Hawthorne, S., Gorecki, C., Sorensen, J., Steadman, E., Harju, J., Melzer, S., 2013. Hydrocarbon mobilization mechanisms from upper middle and lower bakken reservoir rocks exposed to CO_2. In: SPE 167200, SPE Unconventional Resources Conference-Canada, 5-7 November, Calgary, Alberta, Canada. https://doi.org/10.2118/167200-MS.

He, L., Shen, P., Liao, X., Gao, Q., Wang, C., Li, F., 2015. Study on CO_2 EOR and its geological sequestration potential in oil field around Yulin city. J. Petrol. Sci. Eng. https://doi.org/10.1016/j.petrol.2015.06.002.

Hu, J., Sun, R., Zhang, Y., 2020. Investigating the horizontal well performance under the combination of micro-fractures and dynamic capillary pressure in tight oil reservoirs. Fuel. https://doi.org/10.1016/j.fuel.2020.117375.

Ji, H.L., Lee, K.S., 2019. Investigation of asphaltene-derived formation damage and nano-confinement on the performance of CO_2 huff-n-puff in shale oil reservoirs. J. Petrol. Sci. Eng. https://doi.org/10.1016/j.petrol.2019.106304.

Li, B., Bai, H., Li, A., Zhang, L., Zhang, Q., 2019a. Experimental investigation on influencing factors of CO_2 huff and puff under fractured low permeability conditions. Energy Sci. Eng. https://doi.org/10.1002/ese3.376.

Li, L., Su, Y., Hao, Y., Zhan, S., Lv, Y., Zhao, Q., Wang, H., 2019b. A comparative study of CO_2 and N_2 huff-n-puff EOR performance in shale oil production. J. Petrol. Sci. Eng. https://doi.org/10.1016/j.petrol.2019.06.038.

Li, X., Yang, Z., Lei, Q., et al., 2019c. Microscopic Reservoir Characteristic and Effective Development Technology for Low-Permeability and Tight Reservoir. Petroleum Industry Press, Beijing (in Chinese).

Liu, X., Zhang, D., 2019. A review of phase behavior simulation of hydrocarbons in confined space: implications for shale oil and shale gas. J. Nat. Gas Sci. Eng. https://doi.org/10.1016/j.jngse.2019.102901.

Liu, Y., Li, H.A., Okuno, R., 2018. Phase behavior of N_2/n-C_4H_{10} in a partially confined space derived from shale sample. J. Petrol. Sci. Eng. https://doi.org/10.1016/j.petrol.2017.10.061.

Ma, Q., Yang, S., Lv, D., Wang, M., Chen, J., Kou, G., Yang, L., 2019. Experimental investigation on the influence factors and oil production distribution in different pore sizes during CO_2 huff-n-puff in an ultra-high-pressure tight oil reservoir. J. Petrol. Sci. Eng. https://doi.org/10.1016/j.petrol.2019.04.012.

Pu, W., Du, D., Wang, S., Zeng, L., Feng, R., Memon, S., Sarout, J., Sarmadivaleh, M., Xie, Q., Varfolomeev, M.A., 2020. Experimental study of CO_2 huff-n-puff in a tight conglomerate reservoir using true triaxial stress cell core fracturing and displacement system: a case study. J. Petrol. Sci. Eng. https://doi.org/10.1016/j.petrol.2020.108298.

Song, Z., Song, Y., Li, Y., Bai, B., Hou, J., 2020. A critical review of CO_2 enhanced oil recovery in tight oil reservoirs of North America and China. Fuel. https://doi.org/10.1016/j.fuel.2020.118006, 2020.

Shen, Z., James, J.S., 2018. Experimental and numerical study of permeability reduction caused by asphaltene precipitation and deposition during CO_2 huff and puff injection in Eagle Ford shale. Fuel. https://doi.org/10.1016/j.fuel.2017.09.047.

Sun, L., Zou, C., Jia, A., Wei, Y., Guo, Z., 2019. Development Characteristics and Orientation of Tight Oil and Gas in China. Petroleum Exploration and Development. https://doi.org/10.1016/S1876-3804(19)60264-8.

Sun, R., Yu, W., Xu, F., Pu, H., Miao, J., 2018. Compositional simulation of CO_2 Huff-n-Puff process in Middle Bakken tight oil reservoirs with hydraulic fractures. Fuel. https://doi.org/10.1016/j.fuel.2018.09.113.

Syed, F., Neghabhan, S., Zolfaghari, A., Dahaghi, A., 2020. Numerical validation of asphaltene precipitation and deposition during CO_2 miscible flooding. Petrol. Res. https://doi.org/10.1016/j.ptlrs.2020.04.002.

Tang, M., Zhao, H., Ma, H., Lu, S., Chen, Y., 2017. Study on CO_2 huff-n-puff of horizontal wells in continental tight oil reservoirs. Fuel. https://doi.org/10.1016/j.fuel.2016.10.027.

Tang, Y., Tang, J., Liu, Q., Wang, Y., He, Y., 2020. Review on phase behavior in tight porous media and microscopic flow mechanism of CO_2 huff-n-puff in tight oil reservoirs. Geofluids. https://doi.org/10.1155/2020/8824743.

Tang, X., Li, Y., Han, X., Zhou, Y., Zhan, J., Xu, M., Zhou, R., Cai, K., Chen, X., Wang, L., 2021. Dynamic Characteristics and Influencing Factors of CO_2 Huff and Puff in Tight Oil Reservoirs. Petroleum Exploration and Development. https://doi.org/10.1016/S1876-3804(21)60079-4.

Wang, H., Liao, X., Zhao, X., 2015. Study of tight oil reservoir flow regimes in different treated horizontal well. J. Energy Inst. https://doi.org/10.1016/j.joei.2014.05.002.

Wang, L., Tian, Y., Yu, X., Wang, C., Yao, B., Wang, S., Winterfeld, P.H., Wang, X., Yang, Z., Wang, Y., 2017. Advances in improved/enhanced oil recovery technologies for tight and shale reservoirs. Fuel. https://doi.org/10.1016/j.fuel.2017.08.095.

Wang, Y., Hou, J., Tang, Y., 2016. In-situ CO_2 generation huff-n-puff for enhanced oil recovery: laboratory experiments and numerical simulations. J. Petrol. Sci. Eng. https://doi.org/10.1016/j.petrol.2016.04.002.

Yu, H., Lu, X., Fu, W., Wang, Y., Xu, H., Xie, Q., Qu, X., Lu, J., 2020. Determination of minimum near miscible pressure region during CO_2 and associated gas injection for tight oil reservoir in Ordos Basin, China. Fuel. https://doi.org/10.1016/j.fuel.2019.116737.

Zanganeh, P., Dashti, H., Ayatollahi, S., 2018. Comparing the effects of CH_4, CO_2, and N_2 injection on asphaltene precipitation and deposition at reservoir condition: a visual and modeling study. Fuel. https://doi.org/10.1016/j.fuel.2018.01.005.

Zanganeh, P., Dashti, H., Ayatollahi, S., 2015. Visual investigation and modeling of asphaltene precipitation and deposition during CO_2 miscible injection into oil reservoirs. Fuel. https://doi.org/10.1016/j.fuel.2015.07.063.

Zhao, X., Yang, Z., Lin, W., Xiong, S., Wu, Z., 2019. Study on pore structures of tight sandstone reservoirs based on nitrogen adsorption, high-pressure mercury intrusion, and rate-controlled mercury intrusion. J. Energy Resour. Technol. https://doi.org/10.1115/1.4043695.

Zheng, T., Liu, X., Yang, Z., Luo, Y., Zhao, X., 2021a. Identification of seepage mechanisms for natural gas huff-n-puff and flooding processes in hydrophilic reservoirs with low and ultra-low permeabilities. J. Energy Resour. Technol. https://doi.org/10.1115/1.4048526.

Zheng, T., Yang, Z., Liu, X., Luo, Y., Xiao, Q., Zhang, Y., Zhao, X., 2021b. Understanding immiscible natural gas huff-N-puff seepage mechanism in porous media: a case study of CH_4 huff-N-puff by laboratory numerical simulations in chang-7 tight core. Nat. Resour. Res. https://doi.org/10.1007/s11053-021-09836-2.

Zhou, X., Yuan, Q., Rui, Z., Wang, H., Feng, J., Zhang, L., Zeng, F., 2019. Feasibility study of CO2 huff 'n' puff process to enhance heavy oil recovery via long core experiments. Appl. Energy. https://doi.org/10.1016/j.apenergy.2018.12.007.

Zhu, C., Guo, W., Wang, Y., Li, Y., Gong, H., Xu, L., Dong, M., 2020. Experimental study of enhanced oil recovery by CO2 huff-n-puff in shales and tight sandstones with fractures. Petrol. Sci. https://doi.org/10.1007/s12182-020-00538-7.

Zhu, J., Chen, J., Wang, X., Fan, L., Nie, X., 2021. Experimental investigation on the characteristic mobilization and remaining oil distribution under CO_2 huff-n-puff of Chang 7 continental shale oil. Energies. https://doi.org/10.3390/en14102782.